Tantalum and aluminum co-doped iron oxide as a robust photocatalyst for water oxidation

Yanqing Cong, Meimei Chen, Te Xu, Yi Zhang, Qi Wang*

School of Environmental Science and Engineering, Zhejiang Gongshang University, Hangzhou 310012, China

ABSTRACT

Efficient and stable photocatalysts for water oxidation are highly sought after in the field of photoelectrochemical (PEC) water splitting. Herein, a new type of tantalum and aluminum co-doped iron oxide (Ta/Al-Fe$_2$O$_3$) material was fabricated by a simple drop coating method. XPS analysis suggests that Ta and Al were successfully co-doped into Fe$_2$O$_3$ and Ta can greatly influence the chemical environment of Al and O on the surface of catalyst. The resultant optimum (0.25%)Ta/(10%)Al-Fe$_2$O$_3$ film presented excellent enhanced PEC activity and photostability. A 15 times higher photocurrent density as well as two times higher incident-photon-to-current efficiency (IPCE, 430 nm) can be clearly observed relative to (10%)Al-Fe$_2$O$_3$ at 0.35 V vs. Ag/AgCl. The dramatic enhanced PEC and IPCE performance are attributed to mixed effects induced by tantalum doping, such as positive shift of flat band potential (ca. 50 mV), a reduction in anodic overpotential for water oxidation and greatly reduced charge transfer resistance, which eventually facilitate more efficient separation and easier transfer of photogenerated electron–hole pairs. The highly improved visible light activity and film stability indicate that tantalum and aluminum co-doped iron oxide will be a promising semiconductor for water oxidation.

© 2013 Elsevier B.V. All rights reserved.

1. Introduction

Photoelectrochemical (PEC) water splitting into hydrogen and oxygen has been regarded as one of the most promising strategy for collecting and storing the harvested solar energy on a global scale [1–4]. However, it still remains a great challenge to develop an efficient semiconductor electrode under visible light irradiation which accounts up to ca. 43% sunlight [5]. Basically, the most promising photoelectrodes should have the properties of appropriate band edges for targeted reactions, good cycling stability, environmental friendliness and low cost. In addition, a simple and inexpensive electrode preparation method is also pivotal for potential application.

Among various semiconductors, Fe$_2$O$_3$ has emerged as a strong candidate in the photoassisted water oxidation reaction since it has favorable band gap (2.0–2.2 eV), the necessary valence band position for oxygen evolution, stability against corrosion, nontoxicity and ample abundance [6]. The theoretical maximum solar-to-hydrogen efficiency is as high as 15% when Fe$_2$O$_3$ is used as a photoanode [7]. However, these favorable characteristics are balanced against its low conductivity, a miserably short excited state lifetime, a short hole diffusion length, high recombination

of photogenerated electron–hole pairs and the need of a large applied potential for producing a photocurrent [6,8,9].

Considerable efforts have been focused on improving the PEC activities of Fe$_2$O$_3$ by incorporating noble metals into Fe$_2$O$_3$. For example, Pt, Pd, Au or Ag [10–13] doped Fe$_2$O$_3$ all exhibited significantly enhancement of PEC performance due to suppressed recombination and promoted transportation of photogenerated charge carriers by the incorporation of noble metals. Incorporating metal cations such as Si, Ti, Al, Mo, Cr, Nb [14–22] has also been proven to be effective methods for increasing carrier concentrations and hencing conductivity. Meanwhile, surface modifications with water oxidation catalysts such as IrO$_2$, Co-phosphate or Co nanoparticles (NPs) [23–28] would improve reaction kinetics and reduce overpotentials. However, previous researches concern much on single substrate modification, little attention has been paid to photoelectrodes with simultaneously two substances modification, which were found to exhibit potentially more excellent PEC performance [29]. For example, Jang et al. screened Ag for hematite with a scanning electrochemical microscopy and found that 50% Ag–50% Fe with addition of 2% Sn achieved an optimum photocurrent response as that compared to Ag–Fe binary oxides [13]. Sartoretti et al. reported that Fe$_2$O$_3$ doped with Al/Ti or Zn/Ti increased the hole diffusion length and consequently exhibited more attractive PEC activity than Fe$_2$O$_3$ thin films [30]. Despite wide attempt to overcome the intrinsic limitations of Fe$_2$O$_3$, the efficiency of Fe$_2$O$_3$ semiconductor electrodes for PEC water splitting still falls far from satisfactory and fabricating ternary iron

---

oxides offers immense potential to achieve a robust photocatalyst for PEC water oxidation.

In this study, a new type of ternary iron oxides was developed as a robust water oxidation catalyst by introducing tantalum and aluminum cations into Fe_2O_3 to replace iron via simple drop coating method. The structural and PEC performance of $Al-Fe_2O_3$ and $Ta/Al-Fe_2O_3$ electrodes were investigated systematically under visible and UV-visible (UV–vis) light irradiation. It was found that a very small amount of Ta (0.25%) co-doping will lead to a huge upgrade on the PEC activity. The resultant optimum ternary $Ta/Al-Fe_2O_3$ electrode showed a 15 times higher photocurrent density relative to binary $Al-Fe_2O_3$ electrode. To the best of our knowledge, this is the first report of tantalum and aluminum co-doped into Fe_2O_3 with extremely high PEC performance.

2. Experimental

2.1. Chemicals

Tantalum (V) chloride ($TaCl_5$) (99.9% purity) was purchased from J&K Scientific Ltd. (Beijing, China). Aluminum chloride hexahydrate ($AlCl_3 \cdot 6H_2O$) (99.99% purity) and Cobalt (II) acetate tetrahydrate ($Co(CH_3COO)_2 \cdot 4H_2O$) (99.9% purity) were obtained from Aladdin Chemistry Co., Ltd. (Shanghai, China). Ferric nitrate nonahydrate ($Fe(NO_3)_3 \cdot 9H_2O$) (98.5% purity), Ethanol (99.7% purity), Ethylene glycol (99.5% purity) and Ammonia (25% purity) were available from Chengdu Kelong Chemical Reagent Co., Ltd. (Sichuan, China). All chemicals used in this study were analytical grade reagents and were used as received without further purification.

2.2. Synthesis of $Ta/Al-Fe_2O_3$, $Al-Fe_2O_3$ and Fe_2O_3 films

A simple drop coating method was used to prepare the photocatalyst films. The procedures are as follows: $Fe(NO_3)_3 \cdot 9H_2O$, $AlCl_3 \cdot 6H_2O$, $TaCl_5$ were introduced in ethylene glycol at 10 mM to prepare metal precursor solutions. $Al-Fe_2O_3$ solution was achieved with various Al/Fe molar ratio (0%, 5%, 8%, 10%, 12%, 15%, 20%) by addition of $AlCl_3 \cdot 6H_2O$ precursor solution into $Fe(NO_3)_3 \cdot 9H_2O$ precursor solution. $Ta/Al-Fe_2O_3$ solution was obtained by adding $TaCl_5$ precursor solution into $Al-Fe_2O_3$ solution (molar ratio of Al/Fe was 10%) with various molar ratio of Ta/Fe (0%, 0.1%, 0.25%, 0.5%, 2%). Then the as-prepared solutions (30 μL) were pipetted onto F-doped tin oxide (FTO, Nippon Sheet Glass, Japan) substrate (10 mm × 10 mm) and dried in a vacuum oven at 80 °C. After repeating this procedure 4 times, the films were heated at 500 °C for 3 h. For Fe_2O_3 films, 10 mM $Fe(NO_3)_3 \cdot 9H_2O$ solution was prepared. The other conditions for drop coating and heat treatment were identical to those of $Al-Fe_2O_3$ and $Ta/Al-Fe_2O_3$ films.

2.3. Preparation of Co_3O_4 NPs as oxygen evolution catalysts

Co_3O_4 NPs were synthesized based on a literature process [28]. Briefly, $Co(CH_3COO)_2 \cdot 4H_2O$ (0.5 g) was dissolved in ethanol (25 mL) and ammonia (25%, 2.5 mL) was added under vigorous stirring for 10 min, forming a homogeneous viscous slurry. The suspension was transferred into an autoclave (50 mL), sealed, maintained at 150 °C for 3 h and then cooled to room temperature. $Ta/Al-Fe_2O_3$, $Al-Fe_2O_3$ films were immersed in the resulting freshly prepared Co_3O_4 NPs solution (2 mL) for 3 h, washed with distilled water and then dried in air to fabricate $Ta/Al-Fe_2O_3/Co_3O_4$ and $Al-Fe_2O_3/Co_3O_4$ films.

2.4. PEC experiments

PEC experiments were conducted in a three-electrode configuration equipped with an Ag/AgCl reference electrode and a platinum counter electrode at room temperature. A potentiostat (CH Instruments, model 660D) was used to perform electrochemical measurements. The electrodes were irradiated with light from a Xe lamp fitted with a cut-off filter to achieve visible light and the resulting incident intensity was ca. 100 mW cm^{-2}. All films were back-illuminated through the FTO glass. Photocurrents were measured in 0.1 M Na_2SO_4 with 0.1 M Na_2SO_3 aqueous solution (pH 9.3) or in 0.2 M NaOH aqueous solution (pH 13.3). IPCE measurements were detected with a Xe lamp fitted with different monochromatic filters (400, 430, 450, 475, 500, 550 nm) combined with a power meter (model FZ-A) in 0.1 M Na_2SO_4 with 0.1 M Na_2SO_3 aqueous solution. Mott–Schottky (M–S) plot was obtained using a potentiostat at frequencies of 500, 1000, 3000 Hz and a peak-to-peak amplitude of 5 mV at each potential in 0.2 M NaOH aqueous solution. Nyquist plots were achieved in 0.2 M NaOH aqueous solution with a frequency range of 100–0.01 Hz and a scan rate of 5 mV s^{-1} under dark and bright conditions.

2.5. Surface characterization

The crystal structures of as-prepared samples were characterized by X-ray diffraction (XRD) with a Phillips PANalytical X'PERT diffractometer using a Cu-Kα radiation source operated at 40 kV and 40 mA. High resolution transmission electron microscopy (HRTEM) (Philips Tecnai 30 FEI TEM at 300 kV) was used to image the morphology and surface structure of the as-prepared films. Scanning electron microscope (SEM) was performed using an S-4700 (II) (Hitachi) to obtain the thickness of the as-prepared films from side views. X-ray photoelectron spectroscope (XPS) was acquired using a Kratos Axis Ultra DLD instrument with a monochromatic Al X-ray source to determine the surface atomic compositions and valance states of the samples. The binding energies of Fe 2p, Al 2p, Ta 4f and O 1s were referenced against the C 1s (284.6 eV). The optical property of the films was conducted on an UV–vis spectrophotometer (Shimadzu, UV–vis 2450).

3. Results and discussions

3.1. PEC Activities of $Ta/Al-Fe_2O_3$ and $Al-Fe_2O_3$ films

Various synthetic conditions were tried to develop the highest active photocatalysts based on Fe_2O_3 under visible light irradiation. In the present study, Ta and Al were co-doped into Fe_2O_3. The PEC activities of the as-prepared films were characterized by linear sweep voltammetry (LSV) method in 0.1 M Na_2SO_4 with 0.1 M Na_2SO_3 aqueous solution (pH 9.3) under visible light ($\lambda > 420$ nm) irradiation. Na_2SO_4 served as the electrolyte and Na_2SO_3 served as a sacrificial electron donor to consume the photoinduced holes at the semi-conductor/electrolyte interface. Since sulfite oxidation was much easier than water oxidation, higher photocurrents could be obtained in 0.1 M Na_2SO_4 with 0.1 M Na_2SO_3 aqueous solution for the same photocatalysts. Thus, the minor difference in PEC activities among various Al/Fe and Ta/Fe molar ratio photocatalysts based on Fe_2O_3 could be easily found. The photocurrent densities as a function of applied potential (I–V) for different $Al-Fe_2O_3$ films were first tested. As illustrated in Fig. 1a, the photocurrent densities of Fe_2O_3 are greatly enhanced after aluminum doping in the full tested potential range, and the optimum performance is observed at 10% Al/Fe molar ratio. The results are in accordance with the improved activity achieved by electrodeposited aluminum doped hematite [19]. As for $Ta/Al-Fe_2O_3$, different Ta/Fe molar ratio and constant Al/Fe value (10%) were tested. The I–V relationships are depicted in Fig. 1b, and the highest performance can be achieved on (0.25%)Ta/(10%)Al-Fe$_2$O$_3$ film. SEM images of (0.25%)Ta/(10%)Al-Fe$_2$O$_3$ and (10%)Al-Fe$_2$O$_3$ films (see Figure S1
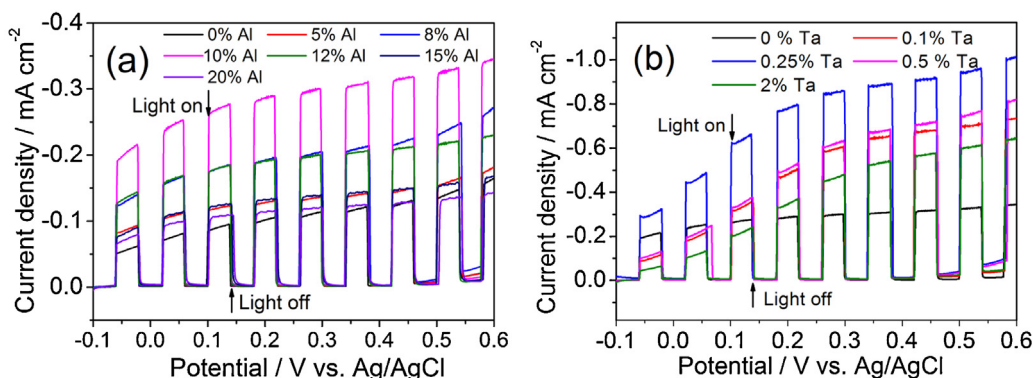
Fig. 1. LSVs of (a) Al-Fe$_2$O$_3$ films with varying molar ratio (Al/Fe) and (b) Ta/(10%)Al-Fe$_2$O$_3$ films with different molar ratio (Ta/Fe) in 0.1 M Na$_2$SO$_4$ with 0.1 M Na$_2$SO$_3$ aqueous solution (pH 9.3) under chopped visible light ($\lambda > 420$ nm) irradiation. Scan rate: 10 mV s^{-1}. Light intensity: 100 mW cm^{-2}.
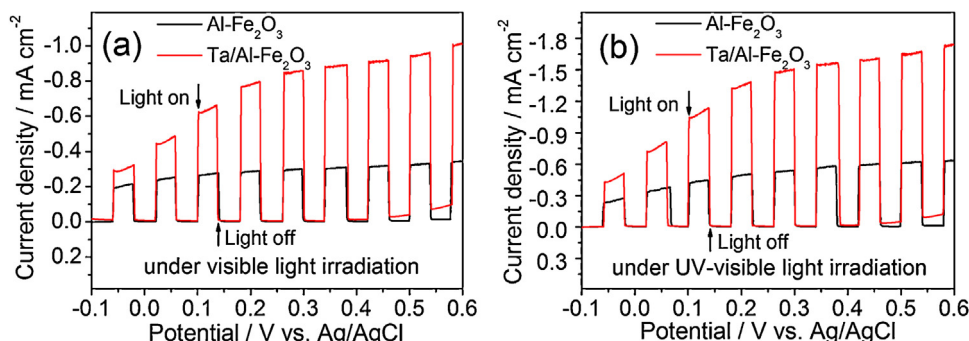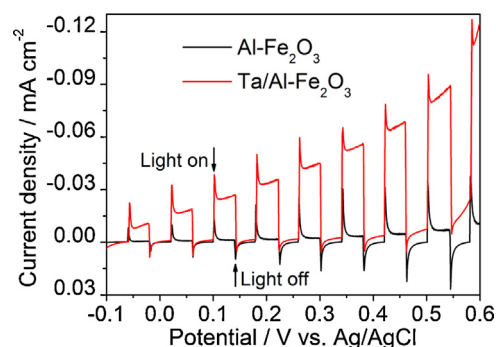

Fig. 2. LSVs of (0.25%)Ta/(10%)Al-Fe$_2$O$_3$ and (10%)Al-Fe$_2$O$_3$ films in 0.1 M Na$_2$SO$_4$ with 0.1 M Na$_2$SO$_3$ aqueous solution (pH 9.3) under chopped (a) visible and (b) UV–vis light irradiation. Scan rate: 10 mV s^{-1}. Light intensity: 100 mW cm^{-2}.

in Supporting Information) indicate that the thickness for Ta/Al-Fe$_2$O$_3$ film (1.95 μm) is quite close to that of Al-Fe$_2$O$_3$ film (1.9 μm). Therefore, it is conceivable that this pronounced enhancement in photocurrent density is due to change in microstructure rather than film thickness induced by Ta co-doped with Al. Therefore, the resultant (0.25%)Ta/(10%)Al-Fe$_2$O$_3$ and (10%)Al-Fe$_2$O$_3$ films were subsequently subjected to further electrochemical, morphological, and crystallographic characterization.

To reveal the improvement of PEC activity caused by Ta loading, LSVs of Ta/Al-Fe$_2$O$_3$ and Al-Fe$_2$O$_3$ films under both visible and UV–vis light irradiation in 0.1 M Na$_2$SO$_4$ with 0.1 M Na$_2$SO$_3$ aqueous solution are presented in Fig. 2. Ta/Al-Fe$_2$O$_3$ film shows an approximately 3 times greater photocurrent density relative to Al-Fe$_2$O$_3$ film at 0.35 V vs. Ag/AgCl. The promotional effect is more noticeable in the higher potential region than in the lower potential region.

To investigate the PEC performance of Ta/Al-Fe$_2$O$_3$ for water oxidation, the corresponding LSVs measurements of Ta/Al-Fe$_2$O$_3$ and Al-Fe$_2$O$_3$ films in 0.2 M NaOH aqueous solution without sacrificial agent were also studied, and the results are shown in Fig. 3. Ta/Al-Fe$_2$O$_3$ film still performs much better than Al-Fe$_2$O$_3$ film. The photocurrent of Ta/Al-Fe$_2$O$_3$ was ca. 15 times higher than that of Al-Fe$_2$O$_3$ film at 0.35 V vs. Ag/AgCl. As a control experiment, single Ta (0.25%) doped Fe$_2$O$_3$ film was also prepared and the photocurrent density is about one-thirds that of (0.25%)Ta/(10%)Al-Fe$_2$O$_3$ at 0.35 V vs. Ag/AgCl. Noticeably, large magnitude of current transients appears for both films associating with either light-on or light-off switching, and larger spikes are observable for Al-Fe$_2$O$_3$ film. Therefore, it can be inferred that the inferior electron–hole pairs recombination processes are involved for both films in PEC measurement, and Ta/Al-Fe$_2$O$_3$ film is assumed to have stronger ability to hinder deleterious recombination reactions.

A rapid oxygen evolution reaction (OER) is difficult to achieve since it involves a four electron, four proton process and occurs with high overpotential even with good electrocatalysts [31]. In order to confirm that the observed current transients in NaOH aqueous solution (Fig. 3) are the exclusive results of O$_2$ evolution but not from the oxidation process of Al-Fe$_2$O$_3$ (or Ta/Al-Fe$_2$O$_3$) films, Co$_3$O$_4$ NPs were loaded onto the surface of both Ta/Al-Fe$_2$O$_3$ and Al-Fe$_2$O$_3$ films. Co$_3$O$_4$ NPs are known to serve as a good electrocatalyst for water oxidation in electrochemical systems. LSVs of Ta/Al-Fe$_2$O$_3$/Co$_3$O$_4$, Ta/Al-Fe$_2$O$_3$, Al-Fe$_2$O$_3$/Co$_3$O$_4$ and Al-Fe$_2$O$_3$ films in 0.2 M NaOH aqueous solution under chopped visible light irradiation were carefully compared. As illustrated in Figure S2 (Supporting Information), Co$_3$O$_4$ NPs modification on both Ta/Al-Fe$_2$O$_3$ and Al-Fe$_2$O$_3$ films significantly improves the photocurrent and suppresses the current spikes under chopped visible light

Fig. 3. LSVs of (0.25%)Ta/(10%)Al-Fe$_2$O$_3$ and (10%)Al-Fe$_2$O$_3$ films in 0.2 M NaOH aqueous solution (pH 13.3) under chopped visible light irradiation. Scan rate: 10 mV s^{-1}. Light intensity: 100 mW cm^{-2}.
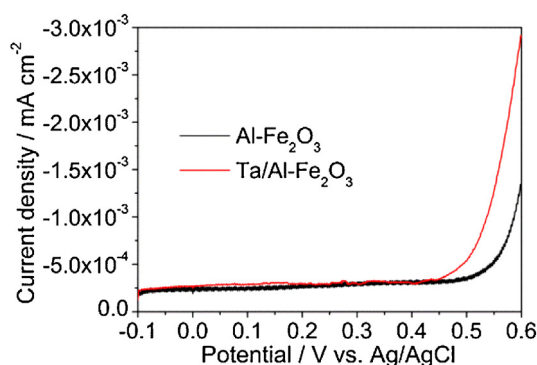
Fig. 4. LSVs of (0.25%)Ta/(10%)Al-Fe$_2$O$_3$ and (10%)Al-Fe$_2$O$_3$ films in 0.2 M NaOH aqueous solution (pH 13.3) in the dark. Scan rate: 10 mV s^{-1}.

irradiation, demonstrating that the observed current transients in Fig. 3 are attributable to water oxidation.

To investigate the surface catalytic nature of photoanode material for O$_2$ evolution, LSVs measurements of Ta/Al-Fe$_2$O$_3$ and Al-Fe$_2$O$_3$ films in the dark near the electrical oxidation of water to O$_2$ in 0.2 M NaOH aqueous solution were performed. The onset potential values can provide important information on the surface catalytic nature [32]. As shown in Fig. 4, the dark response is negligible up to 0.45 V vs. Ag/AgCl for Ta/Al-Fe$_2$O$_3$ film whereas the corresponding value for Al-Fe$_2$O$_3$ film is ca. 0.5 V vs. Ag/AgCl. A 50 mV cathodic shift of onset potential was observed on Ta/Al-Fe$_2$O$_3$ relative to Al-Fe$_2$O$_3$, indicating that the surface of Ta/Al-Fe$_2$O$_3$ film becomes more active and easier for catalytic O$_2$ evolution than that of Al-Fe$_2$O$_3$ film. As a result, the PEC activity was consequently promoted by Ta doping.

3.2. Characterization of Ta/Al-Fe$_2$O$_3$ and Al-Fe$_2$O$_3$ films

XRD analyses were used to identify the crystal phase of Ta/Al-Fe$_2$O$_3$ and Al-Fe$_2$O$_3$ films. Fig. 5a shows the XRD patterns of Ta/Al-Fe$_2$O$_3$, Al-Fe$_2$O$_3$ and pure Fe$_2$O$_3$ films coated on FTO. From the XRD peak analysis, it can be seen that all the samples have comparable crystal structure which is assigned to Fe$_2$O$_3$ (JCPDS 73-0603). It is required to point out that only Fe$_2$O$_3$ crystal structure is observable, implying the absence of other impurity phases. However, when we focus on 2θ peak at 35.6° in a reduced scale range (Fig. 5b), a slight shift of corresponding (1 1 0) plane toward higher angles can be observed for both Ta/Al-Fe$_2$O$_3$ and Al-Fe$_2$O$_3$ films in contrast to pure Fe$_2$O$_3$ film. Similar effects in the full width at half maximum of the XRD peaks were also discovered by Schwertmann [33]. This observation would be explained by the Vegard's lattice

parameter rule which shows a linear decrease of lattice parameter as a function of Al substitution with a change in the lattice constant from 5.0356 to 5.03484 Å. However, no perceivable difference was observed in the XRD patterns of (0.25%)Ta/(10%)Al-Fe$_2$O$_3$ comparing with (10%)Al-Fe$_2$O$_3$ films, which is likely due to low Ta content with respect to Fe.

As a highly surface-sensitive technique, XPS was further used to investigate possible variations induced by Ta doping. Since peaks of Ta 4f could not be detected in the patterns of (0.25%)Ta/Al-Fe$_2$O$_3$ due to very low content of Ta which may be under the detection limit of XPS, (1%)Ta/Al-Fe$_2$O$_3$ film with higher content of Ta were performed for XPS analysis. The electronic states of component elements (Fe, Al, Ta and O) were compared between Ta/Al-Fe$_2$O$_3$ and Al-Fe$_2$O$_3$ films. As illustrated in Fig. 6a, the Fe 2p spectra of both films are quite similar and attributed completely to Fe^{3+}, while no Fe^{2+} shakeup satellite peaks (ca. 715 eV) can be observed. After curve fitting, Fe 2p$_{3/2}$ (four multiplet peaks), Fe 2p$_{3/2}$ satellite, Fe 2p$_{1/2}$ and Fe 2p$_{1/2}$ satellite appear at ca. 709.8–712.3, 718.2, 723.9 and 732.9 eV, respectively. The data of Fe 2p is consistent with previous reports for α-Fe$_2$O$_3$ [21,34], indicating that Fe^{3+} was a primary iron species from α-Fe$_2$O$_3$ in the as-prepared films. Curve fittings of Al 2p for both films are shown in Fig. 6b. The XPS peak of Al 2p was located at 73.3 eV and 73.8 eV in Al-Fe$_2$O$_3$ and Ta/Al-Fe$_2$O$_3$, respectively. A 0.5 eV positive shift of binding energy (BE) for Al 2p can be clearly observed after incorporation of Ta. It is indicative that the BE of Al 2p is very sensitive to the chemical environment and is ascribed to Al^{3+} in Al-substituted Fe$_2$O$_3$ [32]. The result is in accordance with the peak shift achieved by the XRD patterns which was possibly ascribed to substitutional nature of aluminum doping. As shown in Fig. 6c, two doublets at 28.1/26.2 eV and 27.6/25.7 eV corresponding to Ta 4f$_{5/2}$ and Ta 4f$_{7/2}$ can be observed. Since the difference in BE of both doublets is 1.9 eV and the intensity ratio is 3/4, the Ta 4f signals can be assigned to Ta^{5+} [35]. However, the 27.6/25.7 eV doublet do not match well with previous reports where Ta^{5+} in Ta$_2$O$_5$ oxide matrix were usually observed with 28.2/26.3 eV Ta 4f signals. A 0.6 eV negative shift in BE of Ta 4f between the two doublets can be observed. Besides, the doublet Ta 4f are less likely to be ascribed to lower Ta oxidation states such as Ta^{3+} (24.8/26.7 eV), Ta$^+$ (23.9/25.8 eV) and Ta metal (21.7/23.6 eV). Therefore, two kinds of Ta^{5+} exist on the surface of Ta/Al-Fe$_2$O$_3$ and ca. 86.2% Ta was shifted to lower BE. The corresponding positive and negative shift in BE of Al 2p and Ta 4f are indeed observed in the simultaneous incorporation of Ta and Al, indicating that the electron density around Al and Ta are reduced and increased, respectively. Since Ta^{5+} has a higher oxidation state than Al^{3+}, the relative higher electron attracting effect of Ta^{5+} will lead to decreased electron density on Al^{3+} once Ta^{5+} was close to Al^{3+}. Therefore, it can be speculated that Ta^{5+} ions was successfully incorporated into Ta/Al-Fe$_2$O$_3$ film
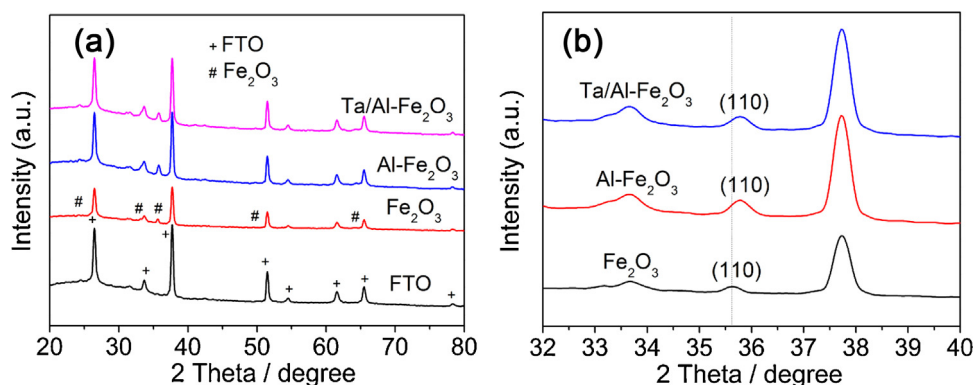
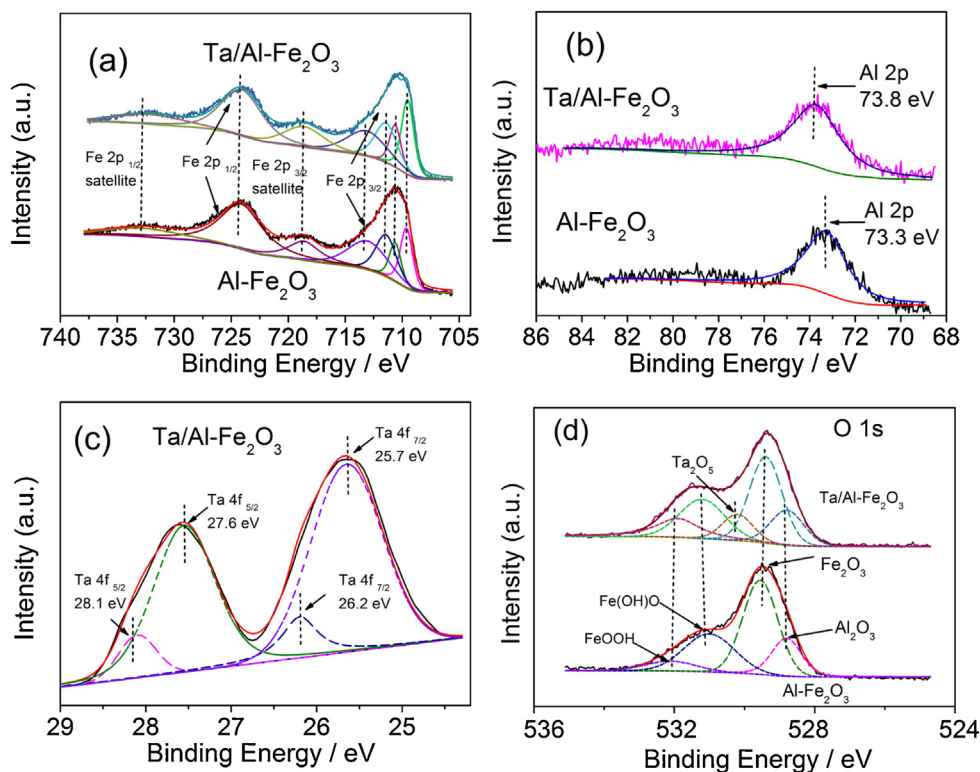**Fig. 5.** XRD patterns of (0.25%)Ta/(10%)Al-Fe$_2$O$_3$, (10%)Al-Fe$_2$O$_3$ and pure Fe$_2$O$_3$ films.

Fig. 6. XPS spectra of (1%)Ta/(10%)Al-Fe$_2$O$_3$ and (10%)Al-Fe$_2$O$_3$ films for (a) Fe 2p$_{3/2}$ and Fe 2p$_{1/2}$, (b) Al 2p (c) Ta 4f$_{5/2}$ and Ta 4f$_{7/2}$, (d) O 1s.

and Ta has a great effect on Al in Ta–Al co-doped Fe$_2$O$_3$. Moreover, the O 1s spectra were also compared. As illustrated in Fig. 6d, four types of O 1s peaks can be observed in Al-Fe$_2$O$_3$ which are ascribed to FeOOH, Fe(OH)O, Fe$_2$O$_3$ and Al$_2$O$_3$, respectively. As for Ta/Al-Fe$_2$O$_3$ film, additional O 1s at 530.3 eV which corresponding to Ta–O bonds in Ta$_2$O$_5$ can be observed [36]. Moreover, the O 1s fraction of FeOOH which was more active in photocatalytic degradation processes [37] increased from 7.2% to 14.5% after incorporation of Ta into Al-Fe$_2$O$_3$. Therefore, it indicates that Ta and Al can be successfully co-doped into Fe$_2$O$_3$ and Ta can greatly influence the chemical environment of Al as well as O on the surface of catalyst.

The morphology and structure of the as-prepared Ta/Al-Fe$_2$O$_3$ film was characterized by HRTEM, and shown in Figure S3 (Supporting Information). A packed arrangement of homogeneous crystallites was observed in Figure S3a and 3b, with the grain size ranging from 90 nm to 150 nm. Figure S3c showed the HRTEM image taken from the area marked by the frame in Figure S3b. From the Fourier-transform images of Figure S3c in top-right and bottom-right inset, polycrystalline could be found and the lattice spacing between two adjacent fringes was very closed, ca. 2.03 Å and 2.05 Å, corresponding to the spacing of {2 0 2} plane of Fe$_2$O$_3$ (JCPDS 73-0603). No clusters of Al or Ta were observed in HRTEM images.

Further investigation on the optical properties of the as-prepared photocatalysts was also performed. Fig. 7 shows the UV–vis spectra of Ta/Al-Fe$_2$O$_3$ and Al-Fe$_2$O$_3$ films. Two absorption bands centered at ca. 400 nm and 540 nm are observed in both films which are consistent with transitions reported in iron oxides previously. The observed peaks are attributed to ligand to metal charge and ligand field transition, respectively [21]. The absorption spectra of the two samples are very similar and an "effective" band gap calculated from the Tauc Plots is ca. 2.18 eV (see Figure S4, Supporting Information). Therefore, the enhanced PEC performance cannot be ascribed to the improved absorption of incident radiation.

3.3. IPCE of Ta/Al-Fe$_2$O$_3$ and Al-Fe$_2$O$_3$ films

IPCE was evaluated to display a more acceptable and standard form of PEC performance on Ta/Al-Fe$_2$O$_3$ and Al-Fe$_2$O$_3$ films by monochromatic irradiation with a Xe lamp attached to a power meter. The photocurrents were measured at certain wavelength in 0.1 M Na$_2$SO$_4$ with 0.1 M Na$_2$SO$_3$ aqueous solution at an applied potential of 0.35 V vs. Ag/AgCl. The value of IPCE can be calculated by the following equation:

$$\text{IPCE(\%)} = 1240 \times \left(\frac{i_{\text{ph}}}{\lambda \cdot P_{\text{in}}} \right) \times 100$$

where i_{ph} is the photocurrent (mA), λ is the wavelength of incident radiation (nm), and P_{in} is the incident light power intensity on the semiconductor electrode at selected wavelength (mW). The results of IPCE as a function of wavelength are illustrated in Fig. 8. It is of high interest that uniformly high IPCE values are observed upon Ta/Al-Fe$_2$O$_3$ film throughout the tested wavelengths, with
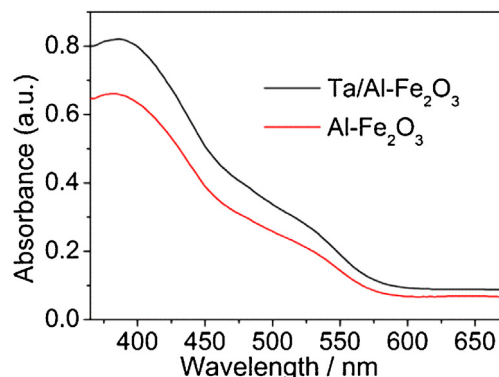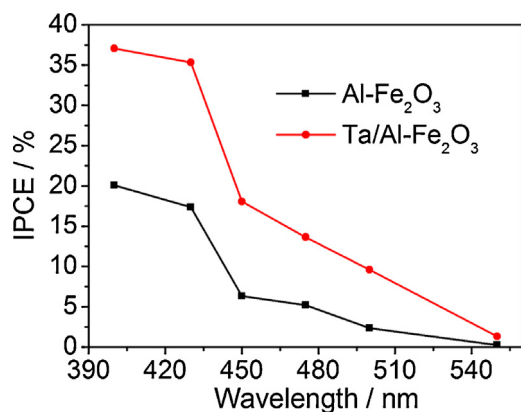

Fig. 7. UV–vis spectra of (0.25%)Ta/(10%)Al-Fe$_2$O$_3$ and (10%)Al-Fe$_2$O$_3$ films.
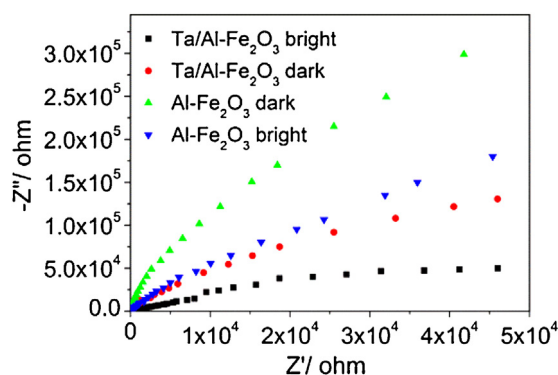
Fig. 8. IPCE plots of (0.25%)Ta/(10%)Al-Fe$_2$O$_3$ and (10%)Al-Fe$_2$O$_3$ films calculated from the photocurrent in 0.1 M Na$_2$SO$_4$ with 0.1 M Na$_2$SO$_3$ aqueous solution (pH 9.3) at an applied potential of 0.35 V vs. Ag/AgCl. Light intensity: 100 mW cm^{-2}.

Fig. 10. Nyquist plots of (0.25%)Ta/(10%)Al-Fe$_2$O$_3$ and (10%)Al-Fe$_2$O$_3$ films in 0.2 M NaOH aqueous solution (pH 13.3) under dark and bright (visible light) conditions with a frequency range of 100–0.01 Hz and a scan rate of 5 mV s^{-1}. Light intensity: 100 mW cm^{-2}.

the value close to 35% at 430 nm and remaining 10% at 500 nm at 0.35 V vs. Ag/AgCl. In contrast, Al-Fe$_2$O$_3$ film exhibits similar but much weaker photocurrent response, and the IPCE values in the whole region are all under 20%. The IPCE onsets of the two samples all generate above 560 nm, regardless of the loading of Ta. The value of band gap can be calculated ca. 2.2 eV that Ta modification does not appreciably change the band gap of Fe$_2$O$_3$. This is consistent with the results achieved from the UV–vis spectra of Ta/Al-Fe$_2$O$_3$ and Al-Fe$_2$O$_3$ films.

3.4. M–S plots and Nyquist plots of Ta/Al-Fe$_2$O$_3$ and Al-Fe$_2$O$_3$ films

Since Ta modification does not affect the bandgap value of Al-Fe$_2$O$_3$, the enhanced PEC and IPCE performance may be ascribed to energetics variation by changing Fermi level and flat band potential. M–S analyses of Ta/Al-Fe$_2$O$_3$ and Al-Fe$_2$O$_3$ films were performed ($1/C_{SC}^2$ vs. E, where C_{SC} is the space charge capacitance of the material) in 0.2 M NaOH aqueous solution at frequencies of 500, 1000 and 3000 Hz in the dark. Fig. 9 shows the M–S plots for Ta/Al-Fe$_2$O$_3$ and Al-Fe$_2$O$_3$ films. The positive slope of each film in M–S plots indicates that it is an n-type semiconductor. The flat band potential shifts positively from ca. −0.8 V for Al-Fe$_2$O$_3$ film to −0.75 V for Ta/Al-Fe$_2$O$_3$ film, which is consistent with observation of the photocurrent onset potential shift (see Figure S5, Supporting Information). All samples are observed to have photocurrent onset potential more positive than the flat band potential. This is probably due to the slow kinetics for water oxidation that results in hole accumulation at the surface, then subsequent surface recombination occurs until sufficiently positive potentials are achieved for appreciable charge transfer across the interface [38]. Since the

doped Ta slightly changed the E_{fb} of Al-Fe$_2$O$_3$ film into a positive direction, while the value of band gap remained unchanged, the oxidative ability toward water oxidation will be improved. As a result, the kinetic for water oxidation can be improved [39], which contributes to enhancing photocurrent of Ta/Al-Fe$_2$O$_3$ vs. Al-Fe$_2$O$_3$ films.

An alternative effect of Ta loading is likely to increase the conductivity of Al-Fe$_2$O$_3$ film, as a result, the charge carrier mobility increased as well as the charge recombination reduced. Electrochemical Impedance Spectroscopy analyses were carried out to check the electrical conductivities of Ta/Al-Fe$_2$O$_3$ and Al-Fe$_2$O$_3$ films. The PEC cell was considered to represent an equivalent circuit of two resistors (solution and electrode) and a single capacitor (electrode) [40]. As represented in the Nyquist plots (Fig. 10), similar semicircles are clearly visible for both Ta/Al-Fe$_2$O$_3$ and Al-Fe$_2$O$_3$ films but with different radii. For Ta/Al-Fe$_2$O$_3$ film, radius of semicircle is smaller than that of Al-Fe$_2$O$_3$ film both under dark and bright conditions, suggesting that decrease in resistance results in increase in conductivity of Ta/Al-Fe$_2$O$_3$ vs. Al-Fe$_2$O$_3$ films.

### 3.5. Stability of Ta/Al-Fe$_2$O$_3$ and Al-Fe$_2$O$_3$ films

The effect of Ta loading on the film photostability was examined by measuring and comparing photocurrent density changes between Ta/Al-Fe$_2$O$_3$ and Al-Fe$_2$O$_3$ films for long time (8 h) visible light irradiation. The experiments were performed in 0.2 M NaOH aqueous solution at 0.35 V vs. Ag/AgCl. As shown in Fig. 11, the photocurrent of Al-Fe$_2$O$_3$ film decreases significantly within a few seconds, then slowly decays and remains ca. 30% photocurrent after 8 h irradiation. This indicated that Al-Fe$_2$O$_3$ film stands poor photostability due to possible anodic photo-corrosion. As for Ta/Al-Fe$_2$O$_3$ film, much smaller transition spikes are observed. Intriguingly, in
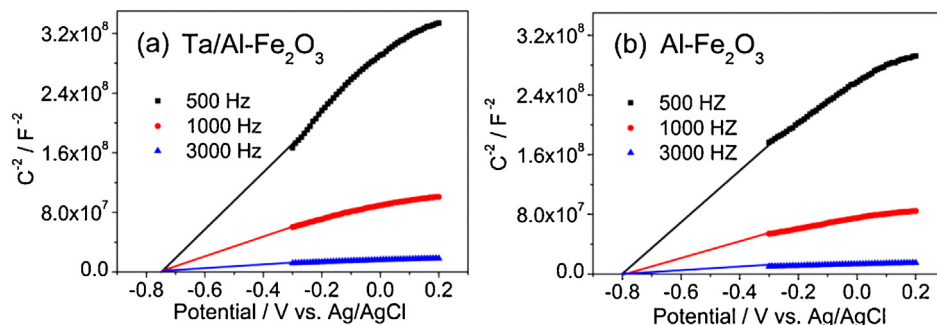
Fig. 9. M–S plots of (a) (0.25%)Ta/(10%)Al-Fe$_2$O$_3$ and (b) (10%)Al-Fe$_2$O$_3$ films in 0.2 M NaOH aqueous solution (pH 13.3) under dark condition with an AC amplitude of 5 mV at each potential.
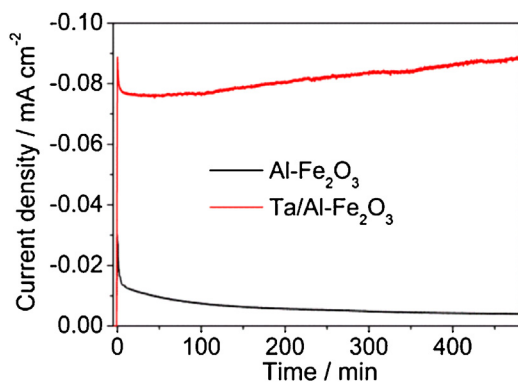
Fig. 11. Photocurrent decay curves measured in 0.2 M NaOH aqueous solution (pH 13.3) under visible light irradiation with a constant potential of 0.35 V vs. Ag/AgCl for (0.25%)Ta/(10%)Al-Fe$_2$O$_3$ and (10%)Al-Fe$_2$O$_3$ films. Light intensity: 100 mW cm^{-2}.
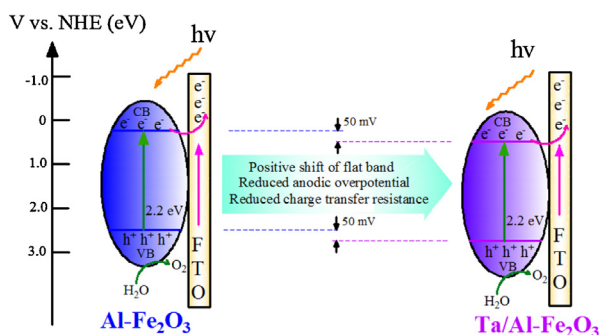
Fig. 12. Schematic of the charge separation and electron transport in (0.25%)Ta/(10%)Al-Fe$_2$O$_3$ and (10%)Al-Fe$_2$O$_3$ films under irradiation.

contrast to photocurrent decay, a steady ascending trend with ca. 15% of increment can be observed on Ta/Al-Fe$_2$O$_3$ film when the test finished. The results demonstrate exceptional promise of Ta/Al-Fe$_2$O$_3$ film for improving photostability as well as photocurrent than Al-Fe$_2$O$_3$ film.

3.6. Possible mechanism

The higher PEC water oxidation activity of Ta/Al-Fe$_2$O$_3$ film is apparently associated with the incorporation of tantalum compared to Al-Fe$_2$O$_3$ film. We rationalize how a very small amount of Ta doping produces the encouraging PEC activity and photostability. A schematic of a tentative mechanism is shown in Fig. 12. The function of Ta can be attributed to different factors: First, the doped Ta slightly changed the E_{fb} of Al-Fe$_2$O$_3$ film into a positive direction, while no significant change of band gap was observed, so the kinetic for water oxidation might be improved. Second, the incorporation of Ta is likely to increase the conductivity of Al-Fe$_2$O$_3$ thus accelerating the mobility of charge carrier and reducing the charge recombination. Third, the value of onset potential which is close to the anodic overpotential for water oxidation is reduced after Ta doping, indicating the surface of Ta/Al-Fe$_2$O$_3$ film becomes more active and easier for catalytic O$_2$ evolution.

4. Conclusions

In this study, we have shown a clear and prominent improvement in photoactivity of a new type ternary iron oxides, Ta/Al-Fe$_2$O$_3$ photoanodes, for solar water-splitting using a simple drop coating method on FTO substrate. XPS analysis suggests that Ta and Al were successfully co-doped into Fe$_2$O$_3$ and Ta can greatly influence the chemical environment of Al and O on

the surface of catalyst. The photocurrent density of the optimum (0.25%)Ta/(10%)Al-Fe$_2$O$_3$ film increased by ca. 15 times relative to (10%)Al-Fe$_2$O$_3$ at 0.35 V vs. Ag/AgCl in NaOH aqueous solution under visible light irradiation. The IPCE of (0.25%)Ta/(10%)Al-Fe$_2$O$_3$ film at 430 nm was ca. 35%, which is 2 times higher than that of (10%)Al-Fe$_2$O$_3$ film under an applied potential of 0.35 V vs. Ag/AgCl. The significant advance in PEC and IPCE performance were attributed to mixed effects induced by tantalum doping, such as positive shift of flat band potential (ca. 50 mV), a reduction in anodic overpotential for water oxidation and greatly reduced charge transfer resistance, which eventually facilitates more efficient separation and easier transfer of photogenerated electron–hole pairs. In a word, the present study highlights that Ta/Al-Fe$_2$O$_3$ is a robust composite semiconductor for PEC water oxidation utilizing visible light.

Acknowledgments

Appendix A. Supplementary data

Supplementary material related to this article can be found, in the online version, at http://dx.doi.org/10.1016/j.apcatb.2013.10.009.

References

[1] T.R. Cook, D.K. Dogutan, S.Y. Reece, Y. Surendranath, T.S. Teets, D.G. Nocera, Chemical Reviews 110 (2010) 6474–6502.
[2] M. Grätzel, Nature 414 (2001) 338–344.
[3] Z.G. Zou, J.H. Ye, K. Sayama, H. Arakawa, Nature 414 (2001) 625–627.
[4] A.J. Bard, M.A. Fox, Accounts of Chemical Research 28 (1995) 141–145.
[5] Q. Li, B.D. Guo, J.G. Yu, J.R. Ran, B.H. Zhang, H.J. Yan, J.R. Gong, Journal of the American Chemical Society 133 (2011) 10878–10884.
[6] Y.J. Lin, S. Zhou, S.W. Sheehan, D.W. Wang, Journal of the American Chemical Society 133 (2011) 2398–2401.
[7] A.B. Murphy, P.R.F. Barnes, L.K. Randeniya, I.C. Plumb, I.E. Grey, M.D. Horne, J.A. Glasscock, International Journal of Hydrogen Energy 31 (2006) 1999–2017.
[8] B. Klahr, S. Gimenez, F. Fabregat-Santiago, T. Hamann, J. Bisquert, Journal of the American Chemical Society 134 (2012) 4294–4302.
[9] J.H. Kennedy, K.W. Frese, Journal of the Electrochemical Society 125 (1978) 709–714.
[10] Y.-S. Hu, A. Kleiman-Shwarstein, A.J. Forman, D. Hazen, J.-N. Park, E.W. McFarland, Chemistry of Materials 20 (2008) 3803–3805.
[11] Y.H. Wei, S.B. Han, D.A. Walker, S.C. Warren, B.A. Grzybowski, Chemical Science 3 (2012) 1090–1094.
[12] J. Zhang, X.H. Liu, L.W. Wang, T.L. Yang, X.Z. Guo, S.H. Wu, S.R. Wang, S.M. Zhang, Journal of Physical Chemistry C 115 (2011) 5352–5357.
[13] J.S. Jang, K.Y. Yoon, X. Xiao, F.-R.F. Fan, A.J. Bard, Chemistry of Materials 21 (2009) 4803–4810.
[14] A. Kay, I. Cesar, M. Grätzel, Journal of the American Chemical Society 128 (2006) 15714–15721.
[15] S. Saremi-Yarahmadi, K.G.U. Wijayantha, A.A. Tahir, B. Vaidhyanathan, Journal of Physical Chemistry C 113 (2009) 4768–4778.
[16] Y.S. Hu, A. Kleiman-Shwarstein, G.D. Stucky, E.W. McFarland, Chemical Communications (2009) 2652–2654.
[17] F. Le Formal, N. Tétreault, M. Cornuz, T. Moehl, M. Grätzel, K. Sivula, Chemical Science 2 (2011) 737–743.
[18] J.S. Jang, J. Lee, H. Ye, F.-R.F. Fan, A.J. Bard, Journal of Physical Chemistry C 113 (2009) 6719–6724.
[19] A. Kleiman-Shwarstein, M.N. Huda, A. Walsh, Y. Yan, G.D. Stucky, Y.-S. Hu, M.M. Al-Jassim, E.W. McFarland, Chemistry of Materials 22 (2010) 510–517.
[20] V.M. Aroutiounian, V.M. Arakelyan, G.E. Shahnazaryan, G.M. Stepanyan, J.A. Turner, O. Khaselev, International Journal of Hydrogen Energy 27 (2002) 33–38.
[21] A. Kleiman-Shwarstein, Y.-S. Hu, A.J. Forman, G.D. Stucky, E.W. McFarland, Journal of Physical Chemistry C 112 (2008) 15900–15907.
[22] V.M. Aroutiounian, V.M. Arakelyan, G.E. Shahnazaryan, G.M. Stepanyan, E.A. Khachaturyan, H. Wang, J.A. Turner, Solar Energy 80 (2006) 1098–1111.
[23] D.K. Zhong, J.W. Sun, H. Inumaru, D.R. Gamelin, Journal of the American Chemical Society 131 (2009) 6086–6087.

[24] T. Kuwabara, E. Tomita, S. Sakita, D. Hasegawa, K. Sone, M. Yagi, Journal of Physical Chemistry C 112 (2008) 3774–3779.
[25] A.J. Esswein, M.J. McMurdo, P.N. Ross, A.T. Bell, T.D. Tilley, Journal of Physical Chemistry C 113 (2009) 15068–15072.
[26] M.W. Kanan, D.G. Nocera, Science 321 (2008) 1072–1075.
[27] Y. Surendranath, M.W. Kanan, D.G. Nocera, Journal of the American Chemical Society 132 (2010) 16501–16509.
[28] Y.M. Dong, K. He, L. Yin, A.M. Zhang, Nanotechnology 18 (2007) 435602.
[29] J.A. Seabold, K.S. Choi, Journal of the American Chemical Society 134 (2012) 2186–2192.
[30] C.J. Sartoretti, B.D. Alexander, R. Solarska, I.A. Rutkowska, J. Augustynski, Journal of Physical Chemistry B 109 (2005) 13685–13692.
[31] H. Ye, H.S. Park, A.J. Bard, Journal of Physical Chemistry C 115 (2011) 12464–12470.
[32] R.L. Spray, K.J. McDonald, K.-S. Choi, Journal of Physical Chemistry C 115 (2011) 3497–3506.
[33] U. Schwertmann, R.W. Fitzpatrick, R.M. Taylor, D.G. Lewis, Clays and Clay Minerals 27 (1979) 105–112.
[34] A.P. Grosvenor, B.A. Kobe, M.C. Biesinger, N.S. McIntyre, Surface and Interface Analysis 36 (2004) 1564–1574.
[35] B. Diaz, J. Swiatowska, V. Maurice, A. Seyeux, E. Harkonen, M. Ritala, S. Tervakangas, J. Kolehmainen, P. Marcus, Electrochimica Acta 90 (2013) 232–245.
[36] E. Atanassova, G. Tyuliev, A. Paskaleva, D. Spassov, K. Kostov, Applied Surface Science 225 (2004) 86–99.
[37] J. He, W.H. Ma, J.J. He, J.C. Zhao, J.C. Yu, Applied Catalysis B: Environmental 39 (2002) 211–220.
[38] S.D. Tilley, M. Cornuz, K. Dr. Sivula, M. Grätzel, Angewandte Chemie International Edition 49 (2010) 6405–6408.
[39] Y.Q. Cong, H.S. Park, H.X. Dang, F.-R.F. Fan, A.J. Bard, C.B. Mullins, Chemistry of Materials 24 (2012) 579–586.
[40] A. Bak, W. Choi, H. Park, Applied Catalysis B: Environmental 110 (2011) 207–215.